

# Impact of compliant electrodes on the dynamics of electromagnetoactive membranes

Ashesh Kumar Patra<sup>a</sup>, Aman Khurana<sup>b,\*</sup>, Deepak Kumar<sup>c</sup>, Prashant Saxena<sup>d</sup>

<sup>a</sup> Department of Mechanical and Industrial Engineering, Indian Institute of Technology Roorkee, Uttarakhand, 247667, India

<sup>b</sup> Department of Mechanical Engineering, Indian Institute of Technology Indore, Madhya Pradesh, 453552, India

<sup>c</sup> Department of Mechanical Engineering, Maulana Azad National Institute of Technology Bhopal, Madhya Pradesh, 462003, India

<sup>d</sup> James Watt School of Engineering, University of Glasgow, Glasgow G12 8LT, UK

## ARTICLE INFO

### Keywords:

Electromagnetoactive polymers  
Pull-in instability  
Compliant electroding  
Electro-magneto-elasticity

## ABSTRACT

The dynamics of electromagnetoactive polymer (EMAP) membranes have attracted much attention recently because of their wide range of modern robotic applications. Such applications majorly centered on how the dynamics of this novel class of membranes are affected by the mechanical behavior of the compliant electrode. This article presents the dynamic modeling and analysis of EMAP membranes, examining how the inertia of the electrode, coupled with its inherent viscoelastic properties, impacts its dynamic performance. Both the compression and suspension stages of the membrane are covered here in broad terms. An Euler–Lagrange equation of motion is implemented to deduce the governing dynamic model equation of the membrane system. The findings of the model solutions provide preliminary insights to characterize the dynamic response, instability analysis, periodic behavior, and resonance properties across varying parameters such as inertia, electric field, magnetic field, and prestress. Moreover, the study also evaluates the periodicity and stability of the nonlinear oscillations using Poincaré maps and phase portraits, facilitating an assessment of quasi-periodic to periodic transitions.

## 1. Introduction

In current trends, soft, multifunctional devices are gradually replacing hard, single-purpose ones. In this change, a growing interest in novel engineering materials for the next generation of electronic devices has recently been focused on the so-called electromagnetoactive polymers, also known as smart elastomers [1–5]. In practice, an electromagnetoactive polymer (EMAP) refers to a smart composite or specialized material class designed to be responsive to both electrical and magnetic stimuli. Such materials can convert magnetic fields into electrical signals and vice versa, which finds usage in sensors, data storage, and energy harvesting [6–8]. Additionally, EMAPs are potentially used in many technical domains where dual responsiveness to electromagnetic fields is advantageous, such as in actuators [9], display screens [10], haptic devices [11], minimum energy structures [12], and other new-generation electronic devices requiring both electrical and magnetic control [13,14].

Fortunately, placing EMAPs in contact is usually unnecessary to activate the polymer with an applied magnetic field. On the other hand, direct contact with compliant electrodes is often requisite for electrical control of such EMAPs, considerably affecting the desired performance

of the device [15,16]. In such active polymers, the term compliant electrode majorly refers to an electrode that does not obstruct the system dynamics of the devices [17]. By assuming that the electrodes are compliant and infinitely thin, the majority of earlier research has ignored the impact of the electrode. A few studies, such as Zhu et al. [18], have examined the resonant behavior of dielectric membranes about electrode mass, asserting that experimental observations indicate electrode mass can sometimes be significantly more than membrane mass. Parallel investigations [17,19–21] have also demonstrated that the electrode material has a significant impact on the dynamic behavior of the elastomer. The elastomer material is often viscoelastic, and therefore the mechanical characteristics are dependent on loading rates [22–25]. An assessment of the performance of such active polymers from a material standpoint has been provided by Romasanta et al. [26]. Very few recent studies [8,27,28] have also explored the dynamic behavior of EMAPs, focusing on their applications in soft robotics and adaptive structures. Research highlights the importance of viscoelastic properties and material damping in EMAP performance and the significant role of electrode inertia in high-frequency actuation, which directly relates to our study. Mathematical models of the mechanics of these elastomers

\* Corresponding author.

E-mail addresses: [amankhurana@iiti.ac.in](mailto:amankhurana@iiti.ac.in) (A. Khurana), [prashant.saxena@glasgow.ac.uk](mailto:prashant.saxena@glasgow.ac.uk) (P. Saxena).

<https://doi.org/10.1016/j.ijnonlinmec.2024.104906>

Received 7 April 2024; Received in revised form 21 August 2024; Accepted 8 September 2024

Available online 17 September 2024

0020-7462/© 2024 The Authors. Published by Elsevier Ltd. This is an open access article under the CC BY license (<http://creativecommons.org/licenses/by/4.0/>).

can be obtained either directly by considering balance laws [29–32] or by variational formulations [33–35]. Large electro- and magneto-mechanically coupled deformation in these soft elastomers can lead to instabilities that have been studied extensively in the literature [27,36–40]. Studies [41–43] also looked into how the rigidities of the electric and magnetic fields affect the nonlinear vibration of cracked magneto-electro-elastic plates. The importance of material inhomogeneity on electromechanical behaviors has been emphasized through such studies of large deformations, pull-in instability, and electrocution in relation to dielectric plates [44,45]. Studies on how permittivity changes during deformation affect electrostriction in elastomers show that the process is not significantly impacted [46]. Furthermore, nonlinearities resulting in friction-type damping and hysteresis effects in dynamic reactions have been discovered to be caused by polarization-electric field interactions in smart plate experiments [44]. Moreover, the vibration characteristics of magneto-electro-elastic nanoplates with functional grading on elastic substrates have been examined, emphasizing the influence of various factors on vibration frequencies [47].

Since electrodes have a major effect on dielectric performance, it is important to take into account how electrodes affect the dynamics of electromagnetoactive polymer membranes. To the best of our knowledge, electrode inertia and its consequent effects on dynamics are not taken into account in dynamical studies of electromagnetoactive polymers. Examining how electrode inertia affects the dynamics of electromagnetoactive polymers is one step towards filling the aforementioned gap in the literature. Furthermore, the analytical solution for the free vibration is obtained, providing more reliable system dynamics. The current study is structured into five distinct sections. Section 2 presents the development of a theoretical model encompassing both compression and suspension phases, articulated in terms of a variable strain energy density function. The dynamic equation governing the motion of the EMAP actuator is formulated using Lagrange's equation, which is grounded on the least action principle. Section 3 delves into the discussion of the variations of static stretch and natural frequency concerning parameter values. A perturbation technique is employed to discern the fundamental responses of the system. The outcomes and discoveries of the investigation are meticulously examined in Section 4. Lastly, Section 5 encapsulates the concluding remarks.

## 2. Problem formulation

The present study focuses on an electromagnetoactive polymer (EMAP) membrane with one end fixed and the other end subjected to a uniaxial load, primarily caused by the mass of an electrode attached at the free end. Notably, the mass of the membrane is considered insignificant compared to the mass of the electrode [20]. Comprehensive analysis is conducted on both suspension and compression phases, supported by schematic representations in Fig. 1, enhancing understanding of the membrane behavior in these conditions. The membrane is assumed to possess hyperelastic properties when subjected to electric and magnetic fields applied vertically, as shown in Fig. 1. The corresponding principal stretches of the membrane as  $\lambda_1$ ,  $\lambda_2$ , and  $\lambda_3$ , representing the extent of deformation along different axes within the material, are defined as:

$$\lambda_1 = \frac{l_1}{L}, \quad \lambda_2 = \frac{l_2}{B}, \quad \lambda_3 = \frac{l_3}{T}, \quad (1)$$

where  $(L, B, T)$  and  $(l_1, l_2, l_3)$  are the set of undeformed and deformed geometrical dimensions of the membrane, respectively. The membrane is assumed to be incompressible and isotropic in nature. For a given incompressible equibiaxial deformation case, the Lagrangian deformation mapping of the EMAP membrane is articulated as:

$$x_1 = \lambda_1 \xi_1 = \lambda^{-0.5} \xi_1, \quad x_2 = \lambda_2 \xi_2 = \lambda^{-0.5} \xi_2, \quad x_3 = \lambda_3 \xi_3 = \lambda \xi_3. \quad (2)$$

To characterize the viscoelastic properties of the membrane, a multiplicative decomposition of the deformation gradient  $\mathbf{F} = \text{Grad } \mathbf{x} = \frac{\partial \mathbf{x}}{\partial \mathbf{X}}$  is incorporated into an elastic part  $\mathbf{F}_s$  and a viscous part  $\mathbf{F}_v$  given by

$$\mathbf{F} = \begin{bmatrix} \lambda^{-0.5} & 0 & 0 \\ 0 & \lambda^{-0.5} & 0 \\ 0 & 0 & \lambda \end{bmatrix} = \begin{bmatrix} \lambda_{s1} & 0 & 0 \\ 0 & \lambda_{s2} & 0 \\ 0 & 0 & \lambda_{s3} \end{bmatrix} \begin{bmatrix} \lambda_{v1} & 0 & 0 \\ 0 & \lambda_{v2} & 0 \\ 0 & 0 & \lambda_{v3} \end{bmatrix}, \quad (3)$$

where  $(\lambda_{s1}, \lambda_{s2}, \lambda_{s3})$  are the elastic stretches and  $(\lambda_{v1}, \lambda_{v2}, \lambda_{v3})$  denote the viscous stretches in the principal directions, respectively. The total energy density ( $\Omega$ ) of the membrane at any point in time is described by the following expression:

$$\Omega = \frac{1}{2} m \mathcal{T}^2 \lambda^2 + AT W_{strain}(\lambda, \lambda_v) - AT E(\lambda) + AT H(\lambda) - 2AT \sigma (\lambda^{-1} - 1) + (-1)^{p+1} mgL \lambda, \quad (4)$$

where  $m$  denotes the overall mass of the membrane and electrodes,  $\sigma$  denotes the equibiaxial pre-stress parameter, while  $g$  represents the acceleration due to gravity. Stretching of the membrane results in the storage of strain energy. This strain energy density is represented by the function  $W_{strain}(\lambda, \lambda_v)$ . Additionally, the work performed by the electrostatic and magnetic forces acting on the membrane is denoted by  $E(\lambda)$ , and  $H(\lambda)$ , respectively. The time derivative of  $\lambda$ , denoted as  $\dot{\lambda}$ , captures the rate of change of the principal stretches over time. It is postulated that the mass of the electrode is uniformly distributed across the cross-sectional area, with the gravitational force exerted at the center of this area. The exponent  $p$  is assigned a value of 0 during the suspension phase and 1 during the compression phase, as depicted in Fig. 1. The system is subject to forces originating from the electromagnetic field, gravitational field, and elastic forces. The system in the present study is non-conservative, meaning that the total energy does not remain constant in motion despite being dependent on position. Differentiating the total energy with respect to time, the equation of motion is obtained as:

$$m \mathcal{T}^2 \dot{\lambda} + AT W'_{strain}(\lambda, \lambda_v) - AT E'(\lambda) + AT H'(\lambda) + 2AT \sigma \lambda^{-2} + (-1)^{p+1} mgL = 0, \quad (5)$$

where,  $W'_{strain}(\lambda, \lambda_v)$ ,  $E'(\lambda)$ , and  $H'(\lambda)$  denote the first differentials of  $W_{strain}(\lambda, \lambda_v)$ ,  $E(\lambda)$ , and  $H(\lambda)$  with respect to the stretch parameter  $\lambda$ , respectively. By examining the aforementioned equation in detail, the corresponding equilibrium condition is deduced as:

$$AT W'_{strain}(\lambda, \lambda_v) - AT E'(\lambda) + AT H'(\lambda) + 2AT \sigma \lambda^{-2} + (-1)^{p+1} mgL = 0. \quad (6)$$

To define the membrane material model as  $W_{strain}(\lambda, \lambda_v)$ , a well-known Gent material model is chosen similar to [8] and the corresponding expression is given by

$$W_{strain}(\lambda, \lambda_v) = \frac{-G j_m}{2} \log \left( 1 - \frac{\lambda_1^2 + \lambda_2^2 + \lambda_3^2 - 3}{j_m} \right) - \frac{\beta G j_m}{2} \log \left( 1 - \frac{\lambda_{s1}^2 + \lambda_{s2}^2 + \lambda_{s3}^2 - 3}{j_m} \right), \quad (7)$$

where  $G$  represents the effective shear modulus of the polymer, while  $\beta$  represents a non-dimensional proportionality constant. The proportionality constant  $\beta$  plays a critical role in dictating the material's viscoelastic behavior by balancing the contributions of the elastic and viscous components. Additionally,  $j_m$  denotes the parameter that delineates the extensional limit of the polymer. With the use of relations in Eq. (3), the principal stretches  $(\lambda_{si})$  in terms of internal variables  $(\lambda_{vi})$  are given by

$$\lambda_{s1} = \lambda^{-0.5} \lambda_v^{0.5}, \quad \lambda_{s2} = \lambda^{-0.5} \lambda_v^{0.5}, \quad \lambda_{s3} = \lambda \lambda_v^{-1}. \quad (8)$$

Substituting the above expressions in Eq. (8) in the energy density expression of Eq. (7), the modified form of the energy density of the membrane is obtained as:

$$W_{strain}(\lambda, \lambda_v) = \frac{-G j_m}{2} \log \left( 1 - \frac{2\lambda^{-1} + \lambda^2 - 3}{j_m} \right)$$

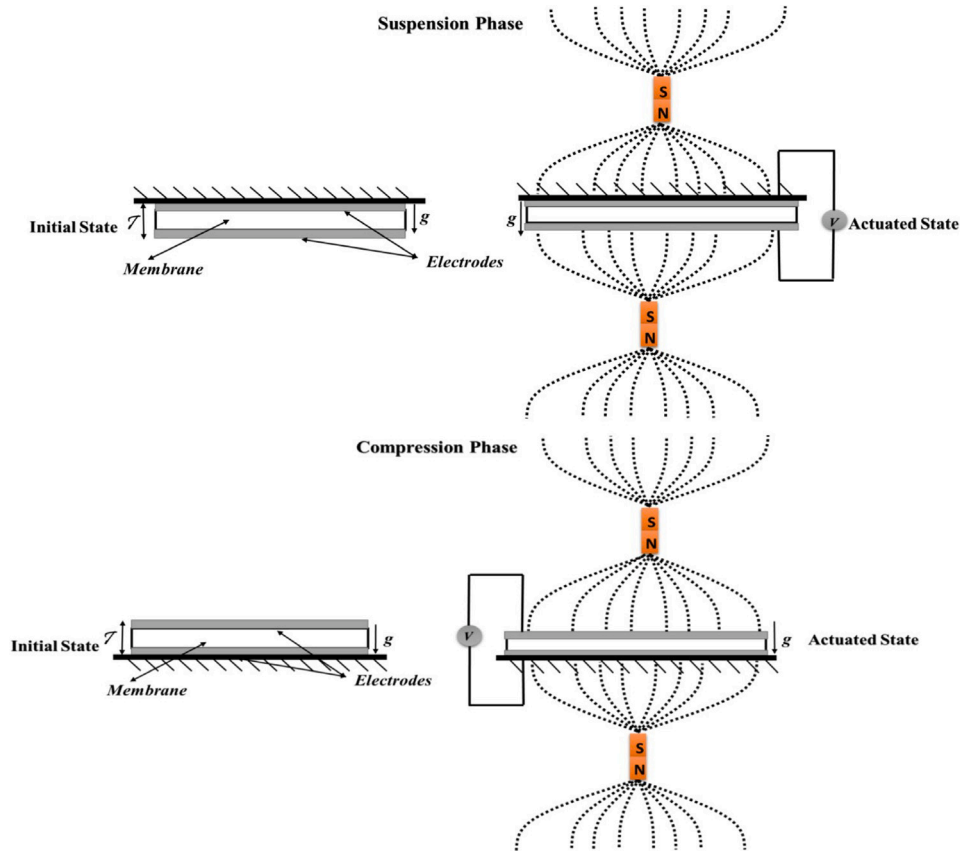


Fig. 1. Schematic diagram for suspension and compression phases.

$$- \frac{\beta G j_m}{2} \log \left( 1 - \frac{2\lambda^{-1}\lambda_v + \lambda^2\lambda_v^{-2} - 3}{j_m} \right). \quad (9)$$

The exertion of external stimuli, namely biaxial prestress, electrostatic, and magnetic forces, is quantified by the following expression, capturing the externally applied load as:

$$\begin{aligned} W_{\text{external}} &= E(\lambda) + H(\lambda) + s(\lambda) = -\frac{1}{2}\epsilon E_o^2 \lambda_1^2 \lambda_2^2 \\ &+ \frac{1}{2}\alpha H_o^2 \lambda_1^{-2} \lambda_2^{-2} - \sigma(\lambda_1 - 1) - \sigma(\lambda_2 - 1) \\ &= -\frac{1}{2}\epsilon E_o^2 2\lambda^{-2} + \frac{1}{2}\alpha H_o^2 \lambda^2 - 2\sigma(\lambda^{-1} - 1). \end{aligned} \quad (10)$$

Consequently, the total energy, denoted as  $U$ , characterizing the EMAP membrane, is given by

$$\begin{aligned} U &= AT \left[ \underbrace{\left[ \frac{-Gj_m}{2} \log \left( 1 - \frac{2\lambda^{-1} + \lambda^2 - 3}{j_m} \right) \right]}_{\text{isotropic equilibrium}} - \underbrace{\left[ \frac{\beta Gj_m}{2} \log \left( 1 - \frac{2\lambda^{-1}\lambda_v + \lambda^2\lambda_v^{-2} - 3}{j_m} \right) \right]}_{\text{isotropic viscous}} \right] \\ &\quad - \underbrace{\left[ \frac{1}{2}\epsilon E_o^2 \lambda^{-2} \right]}_{\text{electrical}} + \underbrace{\left[ \frac{1}{2}\alpha H_o^2 \lambda^2 \right]}_{\text{magnetic}} - \underbrace{\left[ 2\sigma(\lambda^{-1} - 1) \right]}_{\text{prestress}} \\ &\quad + (-1)^{p+1} mgL\lambda. \end{aligned} \quad (11)$$

The total kinetic energy expression for the membrane and compliant electrodes is given by:

$$K = \frac{1}{2} m T^2 \dot{\lambda}^2. \quad (12)$$

To quantify the energy dissipated by the introduced viscous damper in the material model, we rely on a renowned Rayleigh dissipation function denoted as  $D$ , described as [48]:

$$D = AT \left[ \frac{\eta \dot{\lambda}_v^2}{2} \right], \quad (13)$$

where  $\eta$  represents the viscosity parameter of the viscous damper and  $\dot{\lambda}_v$  signifies the time derivative of the principal viscous stretch. For the defined system, the Euler–Lagrange equation of motion resulting from the principle of least action is expressed as [49]:

$$\frac{d}{dt} \left( \frac{\partial Z}{\partial \dot{\lambda}} \right) - \frac{\partial Z}{\partial \lambda} + \frac{\partial D}{\partial \dot{\lambda}} = 0, \quad (14)$$

where  $Z = K - U$ . Substituting all the expressions of kinetic energy  $K$  from Eq. (12) and potential energy  $U$  from Eq. (11) along with the dissipation function  $D$  from Eq. (13) of the EMAP membrane in Eq. (14), the governing equation of motion of the EMAP membrane is deduced as given in Box I. In the above governing equation of motion, the following dimensionless parameters are considered, and the corresponding expressions are given by

$$\tau = t \sqrt{\frac{g}{T}}, \quad \nu = \frac{GA}{mg}, \quad \mu = \frac{A\epsilon E_o^2}{mg}, \quad h = \frac{A\alpha H_o^2}{mg}, \quad S = \frac{\sigma A}{mg}. \quad (16)$$

where  $\tau$  denotes the dimensionless required time period,  $\nu$  represents the dimensionless weight of the electrode applied on the actuator,  $\mu$  denotes the applied dimensionless electric field,  $h$  signifies the applied dimensionless magnetic field, and  $S$  is indicative of the dimensionless mechanical stress. The dynamical behavior of the EMAP membrane undergoing electro-magneto-mechanical deformation is elucidated by the ensuing governing equation:

$$\frac{d^2 \lambda}{d\tau^2} + g(\lambda, \lambda_v : \nu, \mu, h, S) = 0, \quad (17)$$

where,

$$\begin{aligned} g(\lambda, \lambda_v : \nu, \mu, h, S) &= \left\{ -\nu j_m \left[ \frac{\lambda^{-2} - \lambda}{j_m - 2\lambda^{-1} - \lambda^2 + 3} \right] - \nu \beta j_m \left[ \frac{\lambda^{-2}\lambda_v - \lambda\lambda_v^{-2}}{j_m - 2\lambda^{-1}\lambda_v - \lambda^2\lambda_v^{-2} + 3} \right] \right. \\ &\quad \left. + \mu \lambda^{-3} + h\lambda + 2S\lambda^{-2} + (-1)^{p+1} \right\}. \end{aligned} \quad (18)$$

$$\frac{d^2\lambda}{d\tau^2} + \underbrace{\left\{ -\nu j_m \left[ \frac{\lambda^{-2} - \lambda}{j_m - 2\lambda^{-1} - \lambda^2 + 3} \right] - \nu \beta j_m \left[ \frac{\lambda^{-2}\lambda_v - \lambda\lambda_v^{-2}}{j_m - 2\lambda^{-1}\lambda_v - \lambda^2\lambda_v^{-2} + 3} \right] + \mu\lambda^{-3} + h\lambda + 2S\lambda^{-2} + (-1)^{p+1} \right\}}_{g(\lambda, \lambda_v : \nu, \mu, h, S)} = 0. \tag{15}$$

Box I.

In order to evaluate the internal variable  $\lambda_v$ , the evolution equation is formulated utilizing the Euler–Lagrange equation as follows:

$$\frac{d}{dt} \left( \frac{\partial Z}{\partial \dot{\lambda}_v} \right) - \frac{\partial Z}{\partial \lambda_v} + \frac{\partial D}{\partial \dot{\lambda}_v} = 0. \tag{19}$$

With the use of the above-defined Euler–Lagrange equation, the respective evolution equation in dimensionless form is articulated as:

$$\frac{d\lambda_v}{d\tau} \left( \sqrt{\frac{g}{\mathcal{T}}} \right) + \left\{ -\frac{G\beta j_m}{\eta} \left[ \frac{\lambda^2\lambda_v^{-3} - \lambda^{-1}}{j_m - 2\lambda^{-1}\lambda_v - \lambda^2\lambda_v^{-2} + 3} \right] \right\} = 0. \tag{20}$$

Finally, the dimensionless representation of the initial conditions for the defined EMAP membrane system is as follows:  $\left. \frac{d\lambda}{d\tau} \right|_{\tau=0} = 0$ ;  $\lambda|_{\tau=0} = 1$ ;  $\lambda_v|_{\tau=0} = 1$ .

### 3. Small perturbation around equilibrium state

The EMAP membrane attains a condition of equilibrium when the applied electric field ( $\mu$ ) or magnetic field ( $h$ ) remains constant. The equation governing this equilibrium state is expressed by the governing relation (17) as follows:

$$g(\lambda_{eq} : \nu, \mu, h, S) = 0. \tag{21}$$

Herein, the multiple positive roots may be identified for the equilibrium stretch parameter  $\lambda_{eq}$ . However, for the currently defined problem, only one or two of these roots are pertinent. The relationship between the equilibrium stretch ( $\lambda_{eq}$ ) with the normalized electric field ( $\mu$ ) and magnetic field ( $h$ ) is expressed using Eq. (21) as:

$$\mu = \frac{1}{\lambda_{eq}^{-3}} \left\{ \nu j_m \left[ \frac{\lambda_{eq}^{-2} - \lambda_{eq}}{j_m - 2\lambda_{eq}^{-1} - \lambda_{eq}^2 + 3} \right] + \nu \beta j_m \left[ \frac{\lambda_{eq}^{-2} - \lambda_{eq}}{j_m - 2\lambda_{eq}^{-1} - \lambda_{eq}^2 + 3} \right] - h\lambda_{eq} - 2S\lambda_{eq}^{-2} - (-1)^{p+1} \right\}, \tag{22}$$

and

$$h = \frac{1}{\lambda_{eq}} \left\{ \nu j_m \left[ \frac{\lambda_{eq}^{-2} - \lambda_{eq}}{j_m - 2\lambda_{eq}^{-1} - \lambda_{eq}^2 + 3} \right] + \nu \beta j_m \left[ \frac{\lambda_{eq}^{-2} - \lambda_{eq}}{j_m - 2\lambda_{eq}^{-1} - \lambda_{eq}^2 + 3} \right] - h\lambda_{eq}^{-3} - 2S\lambda_{eq}^{-2} - (-1)^{p+1} \right\}. \tag{23}$$

When the membrane experiences a deviation from its static equilibrium stretch ( $\lambda_{eq}$ ) due to a perturbation, the temporal evolution of the membrane stretch may be defined in the following manner:

$$\lambda(\tau) = \lambda_{eq} + \delta(\tau), \tag{24}$$

where  $\delta(\tau)$  denotes an infinitesimal perturbation. The incorporation of the expression derived from Eq. (24) into the governing equation (17) is accomplished via a first-order Taylor series approximation, resulting in:

$$\frac{d^2\delta}{d\tau^2} + \delta \left( \frac{\partial g(\lambda : \nu, \mu, h, S)}{\partial \lambda} \right)_{\lambda=\lambda_{eq}, \lambda_v=1} = 0. \tag{25}$$

The expression for the dimensionless natural frequency is designated as  $\omega_{eq}$  and is derived through Eq. (25) as:

$$\omega_{eq}^2 = \left[ -\nu j_m \left[ \frac{(j_m - 2\lambda_{eq}^{-1} - \lambda_{eq}^2 + 3)(-2\lambda_{eq}^{-3} - 1) - 2(\lambda_{eq}^{-2} - \lambda_{eq})^2}{(j_m - 2\lambda_{eq}^{-1} - \lambda_{eq}^2 + 3)^2} \right] \right]$$

$$- \nu \beta j_m \left[ \frac{(j_m - 2\lambda_{eq}^{-1} - \lambda_{eq}^2 + 3)(-2\lambda_{eq}^{-3} - 1) - 2(\lambda_{eq}^{-2} - \lambda_{eq})^2}{(j_m - 2\lambda_{eq}^{-1} - \lambda_{eq}^2 + 3)^2} \right] - 3\mu^{-4} + h - 4S\lambda_{eq}^{-3} \tag{26}$$

## 4. Results and discussions

This section addresses the analytical findings of the model solution providing preliminary insights to characterize the dynamic response, instability analysis, periodic behavior, and resonance properties across varying parameters such as inertia, electric field, magnetic field, and pre-stress. In the subsequent sub-sections, building upon the established dynamic model of the EMAP membrane as presented in the earlier sections, we undertake a comprehensive examination of the impact of inertia, magnetic field, and pre-stress on the membrane dynamic response in both DC and AC domains. The parametric dependence of the system with respect to natural frequency and static stretch is also investigated. To ensure consistency across all numerical simulations, the material parameters are standardized as follows: the proportionality constant  $\beta = 2$ , in alignment with Refs. [50,51], and the viscosity parameter  $\eta = 5$  is considered throughout the entire numerical investigation in accordance with established conventions [52].

### 4.1. Equilibrium stretch and natural frequency

This sub-section investigates the parametric dependence of static stretch and natural frequency within the system. Static stretch signifies a state of mechanical equilibrium where the net force vanishes. By inserting the expressions for  $W_{strain}(\lambda, \lambda_v)$ ,  $E(\lambda)$ , and  $H(\lambda)$  into Eq. (6), we obtain the equilibrium equation solely in terms of equilibrium stretch  $\lambda_{eq}$ , as presented in Eq. (21). Figs. 2 and 3 visually depict the relationship between static stretch and natural frequency with parameter  $\mu$ , showcasing its variation for both suspension and compression phases across diverse values of  $\nu$  and  $h$ .

It is demonstrably evident that, for a given  $\nu$ , the system maintains a state of equilibrium up to a critical  $\mu$  threshold for both configurations presented. This maximum  $\mu$ , within which stability prevails, exhibits a biphasic response to the augmentation of  $\nu$  in the suspension phase. As illustrated in Fig. 2(a), an initial decrease in the maximum  $\mu$  is followed by a subsequent increase. Fig. 2(b) further reveals a proportional relationship between the system’s natural frequency in a stable state and  $\nu$ . Introducing the electrode’s mass contributes to enhanced stability at higher  $\mu$  values, thus elucidating the rationale behind the observed decrease in the maximum  $\mu$  threshold. Moreover, it can be observed that the  $\omega_{eq}$  decreases in a nonlinear fashion with dimensionless electric field. Notably, all curves intersect at the point  $\lambda_{eq} = 1$ , with some residing within the stable branch and others occupying the unstable branch. With increasing  $\nu$ , the point of unity static stretch transitions into the domain of the stable branch. Within the context of the compression phase, as depicted in Fig. 2(c), stable static stretch persists up to a limiting value of  $\mu$ . Notably, this limiting  $\mu$  exhibits a positive correlation with the increasing value of parameter  $\nu$ . Fig. 2(d) further illustrates a concomitant rise in the natural frequency ( $\omega_{eq}$ ) at the limiting  $\mu$  as  $\nu$  increases. It is crucial to recognize that in this

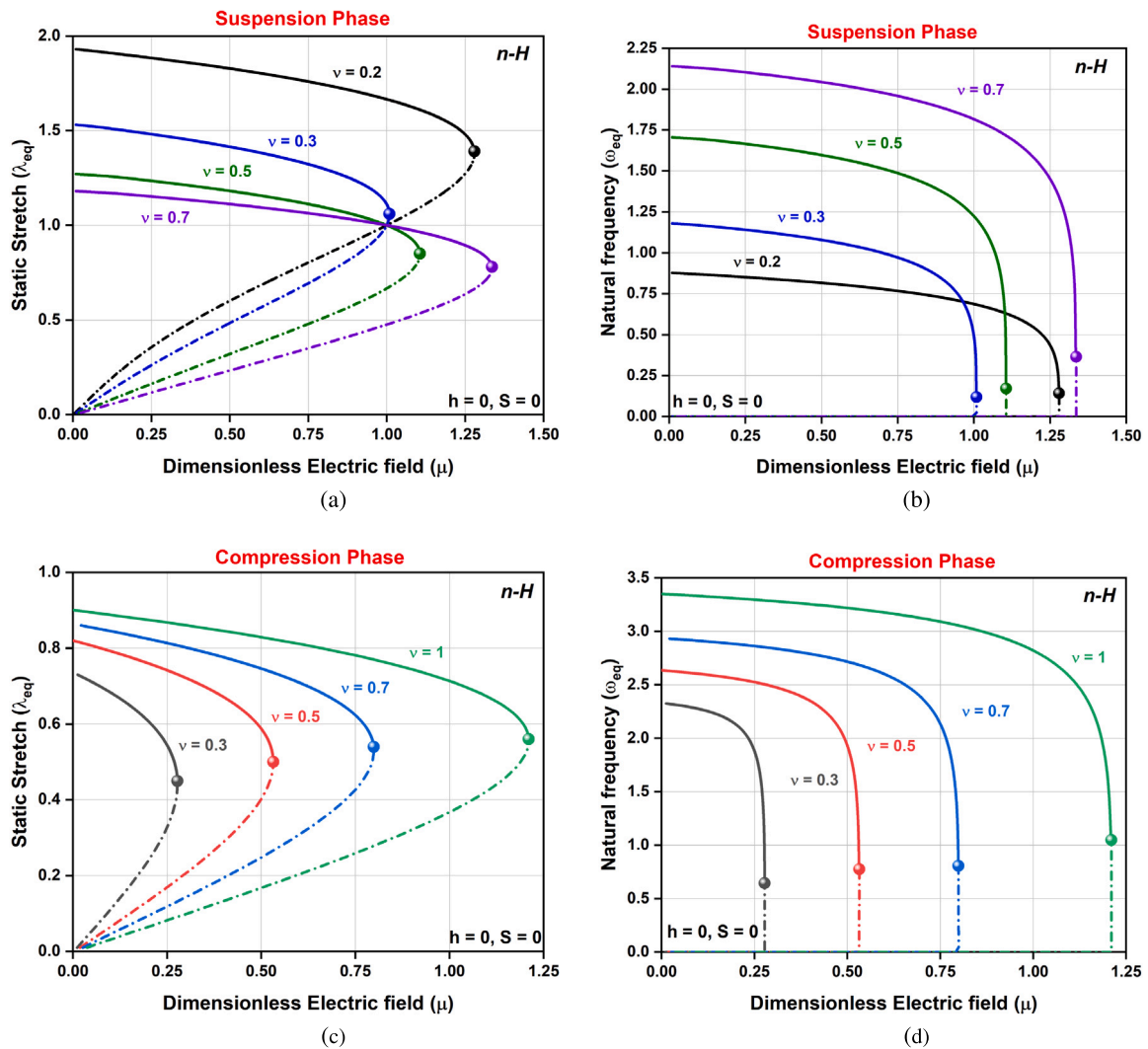


Fig. 2. Variation of static stretch  $\lambda_{eq}$  with dimensionless parameter  $\mu$  in (a) Suspension phase and (b) Compression phase. Variation of natural frequency  $\omega_{eq}$  with dimensionless parameter  $\mu$  in (c) Suspension phase (d) Compression phase.

configuration, the electrode weight applies force in the same direction as the electrode pressure. This, in turn, leads to instability as the electrostatic pressure amplifies with escalating  $\mu$  at a constant  $\nu$ . By critically analyzing the aforementioned figures, it becomes evident that for a fixed  $\mu$  value, instability can manifest across a spectrum of  $\nu$  values.

Fig. 3 visually represents the interplay between static prestretch and natural frequency as a function of the parameter  $\mu$  across a range of  $h$  values, with a constant  $\nu$  of 0.5. Examining both suspension and compression phases in Figs. 3(a–c), it is evident that a stable static stretch endures up to a critical value of  $\mu$ . The discernible negative correlation between this critical  $\mu$  and the escalating parameter  $h$  is noteworthy. The introduction and alignment of the magnetic field play a pivotal role in augmenting stability, offering insight into the rationale underpinning the observed reduction in the maximum  $\mu$  threshold. A nonlinear decrease in the dimensionless electric field's impact on  $\omega_{eq}$  is also observed. Figs. 3(b–d) presents a more nuanced view, revealing that the natural frequency ( $\omega_{eq}$ ) initially rises at the limiting  $\mu$  before declining with increasing  $h$ . Crucially, it is intriguing to observe that the variability in static prestretch and natural frequency is chiefly governed by the implementation of the dimensionless parameter  $h$ . At the same time, there is no reliance on both the mass of the electrodes and the precise orientation of their application, spanning across both

the suspension and compression phases. This intricate interplay becomes evident upon detailed analysis of the figures, highlighting that instability can manifest across a range of  $h$  values for a fixed  $\mu$ .

The subsequent sub-sections delve deeper by solving the non-linear differential equation (15), evolution equation (20), and the stated initial conditions to systematically investigate the impact of various parameters like  $\nu$ ,  $\mu$ ,  $h$ , and  $S$  on the electro-magneto active actuators in both DC and AC dynamic actuation modes.

#### 4.2. DC dynamic response

This sub-section intricately explores the ramifications of diverse dimensionless parameters on the performance of EMAP membrane operating within DC dynamic modes. The study emphasizes maintaining a consistent value for  $\eta$ , expressly set at 5, signifying a designated dimensionless viscosity term. Moreover, the shear modulus of the intelligent composite material remains a constant at  $G = 0.1$  MPa, in alignment with precedent research [53]. The initial length ( $L$ ) of the membrane is presumed to be 0.001 m, and the gravitational acceleration ( $g$ ) adheres to the standard value of  $9.8 \text{ m/s}^2$  [54]. Within this framework, the study systematically scrutinizes the impact of pivotal dimensionless parameters, including  $\nu$ ,  $\mu$ ,  $h$ , and  $S$ , on the dynamic response of the membrane subjected to DC excitation. Through methodically varying these parameters and discerning their collective effects, the objective

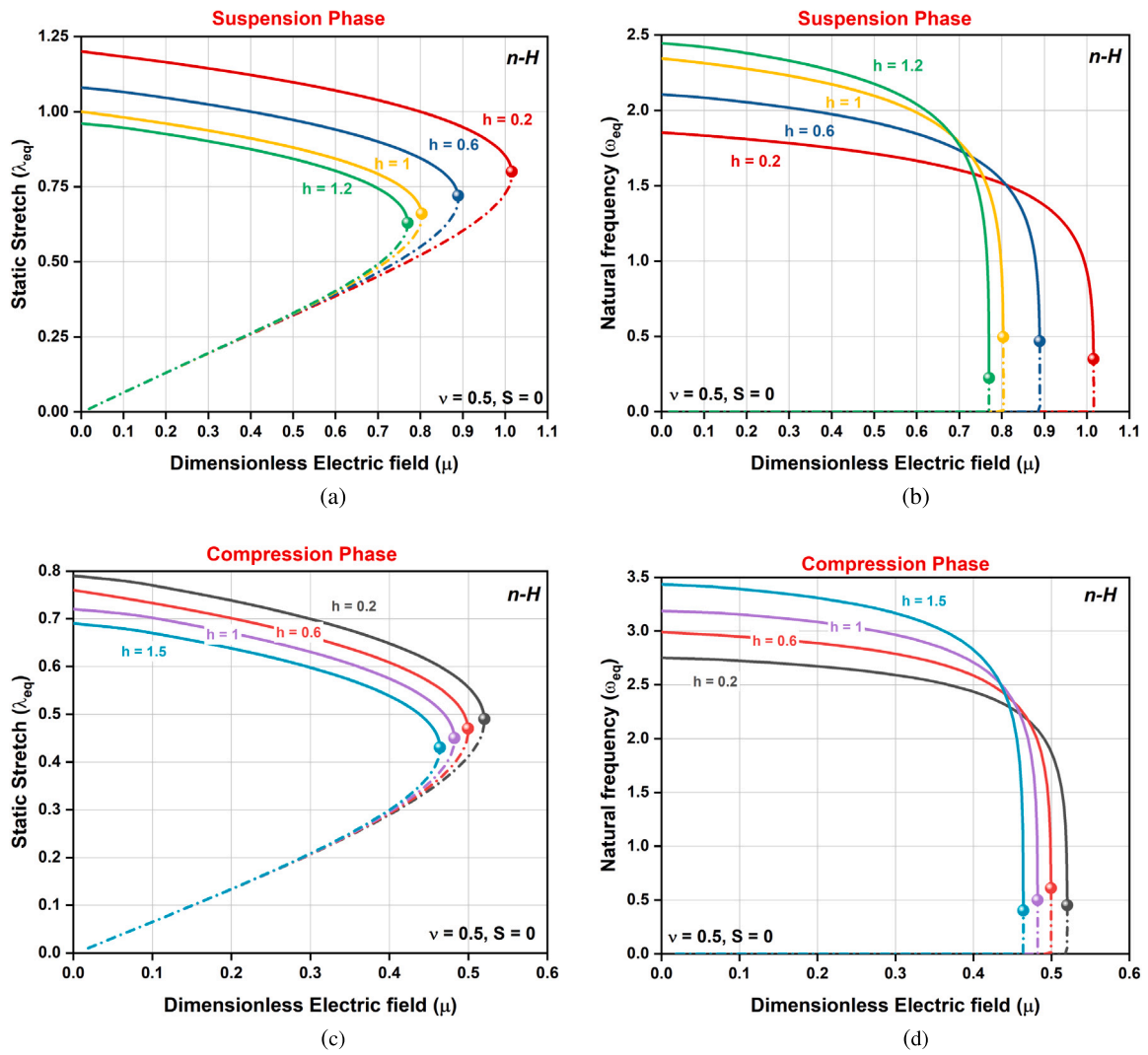


Fig. 3. Variation of static stretch  $\lambda_{eq}$  with dimensionless parameter  $\mu$  in (a) Suspension phase and (b) Compression phase. Variation of natural frequency  $\omega_{eq}$  with dimensionless parameter  $\mu$  in (c) Suspension phase (d) Compression phase.

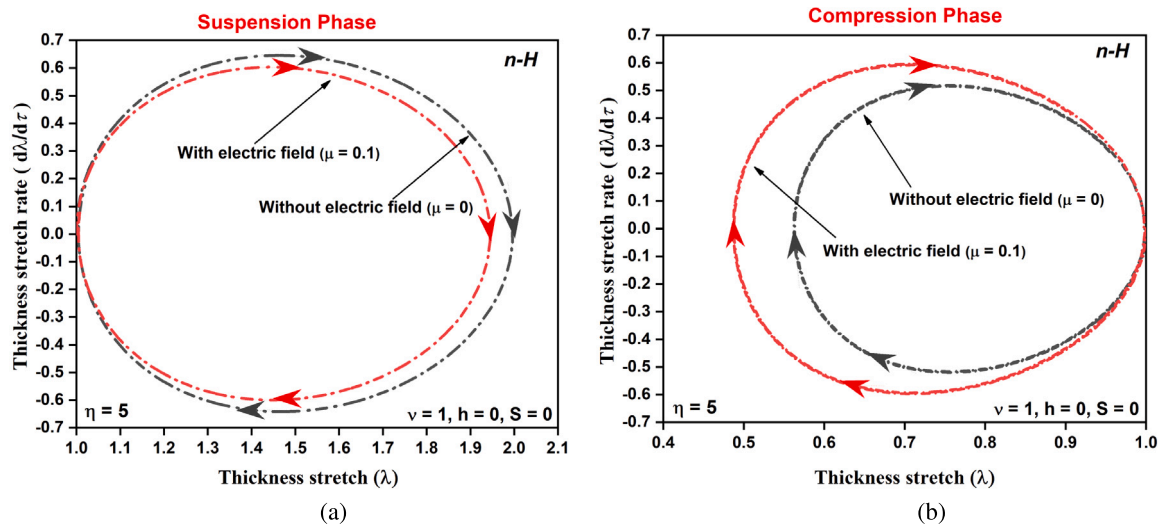


Fig. 4. Comparison of system behavior with and without electric field (a) Suspension phase (b) Compression phase.

is to cultivate a profound comprehension of the intricate dynamics governing the behavior of the membrane in DC modes.

Figs. 4(a) and (b) present a comparative analysis of phase portraits of the membrane in the presence and absence of an electric field.

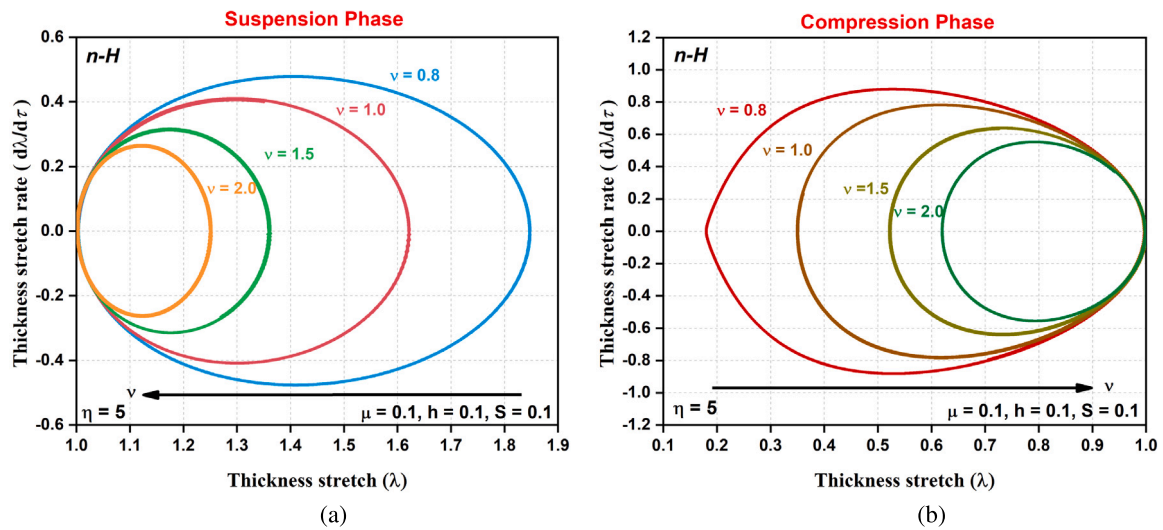


Fig. 5. DC System dynamics with varying  $\nu$  parameter in (a) Suspension phase (b) Compression phase.

A fixed value of  $\nu = 1$  is chosen to ensure a stable system, while other parameters are adjusted accordingly. The analysis leverages the total energy framework, introducing an additional term for the electric field's contribution. Valuable insights are gained by comparing the system's energy with and without the field, focusing on the difference between extreme stretch states. Fig. 4(a) reveals a fascinating phenomenon in the suspension phase. The observed difference between extreme stretches diminishes upon applying the electric field ( $\mu = 0.1$ ). This mathematically translates to a decrease in the overall system energy. This can be attributed to the additional electrical field reducing its potential energy. Conversely, Fig. 4(b) depicts a contrasting scenario in the compression phase. When the electric field is introduced ( $\mu = 0.1$ ), the difference between extreme stretches amplifies, signifying an increase in system energy. This implies that the additional electrical term elevates its potential energy. In essence, the figures elucidate the divergent effects of the electric field on the system's energy depending on the initial phase (suspension or compression). This nuanced understanding underscores the complex interplay between the applied electric field and the inherent dynamics of the membrane system. This trend aligns with the observations in the literature [55].

#### 4.2.1. Effect of the dimensionless stiffness ( $\nu$ ) on DC dynamic response

Initially, Figs. 5(a) and (b) investigate the system behavior under varying dimensionless constants  $\nu$  for fixed values of  $\mu = 0.1$ ,  $h = 0.1$ , and  $S = 0.1$  within both the suspension and compression phases. The analysis reveals a consistent trend across both phases: as  $\nu$  increases, the thickness stretch or the difference between extreme stretches decreases. This observation has crucial implications for the energy of the system. Since the extreme stretches define the potential energy well of the system, their decreasing difference signifies a reduction in the overall system energy. This energy reduction occurs in both the suspension and compression phases, implying that increasing  $\nu$  promotes a more stable and lower-energy state for the system across its operational range.

#### 4.2.2. Effect of the dimensionless magnetic field ( $h$ ) on DC dynamic response

This study further explores the impact of the dimensionless parameter  $h$  on the nonlinear dynamic behavior of EMAP membrane, focusing on its influence on energy transfer. Four distinct values of  $h$  (0.2, 0.4, 0.6, and 0.8) are investigated while maintaining fixed values for  $\nu = 1$ ,  $\mu = 0.1$ , and  $S = 0$ . Introducing a magnetic field adds an extra energy term to the total energy of the system. Comparisons are based on the difference between the two extreme stretch values seen when the membrane is moving to quantify the energy fluctuations.

Fig. 6(a) depicts a notable decrease in the difference between extreme stretches when the magnetic field is applied. This signifies reduced energy stored within the system during the suspension phase. Conversely, Fig. 6(b) demonstrates an opposing trend, where extreme stretch differences increase upon field application. This indicates an augmentation of energy within the system during the compression phase. These contrasting observations highlight the distinct effects of the magnetic field on energy transfer within the EMAP membrane across different phases of its motion. The magnetic field induces energy dissipation during the suspension phase while promoting energy storage during compression.

#### 4.2.3. Effect of dimensionless pre-stress ( $S$ ) on DC dynamic response

Further, Figs. 7(a) and (b) depict the phase portraits of the actuators under varying prestress values. Focusing on a specific set of initial conditions ( $\nu = 1$ ,  $\mu = 0.1$ , and  $h = 0.1$ ), these figures shed light on the DC response of the EMAP membrane when subjected to a constant DC Heaviside electric signal. Fig. 7(a) also portrays a striking observation: an evident decrease in the envelope of the thickness stretch rate with increasing prestress. This translates to reduced energy stored within the system during the suspension phase. This reduction can be attributed to the counteraction of the prestress force against the stretching action induced by the inertia. As a result, less energy is required to deform the actuator against the prestress, leading to a smaller envelope of the stretch rate. However, Fig. 7(b) reveals a contrasting behavior during the compression phase. Unlike the suspension phase, the envelope of the thickness stretch rate increases with increasing prestress. This can be explained by the fact that when the inertia effect reverses direction, the prestress now assists the compression action along with the constant electric and magnetic field. This combined force leads to more significant deformations and, consequently, a higher envelope of the stretch rate. This diverse influence necessitates careful consideration of prestress levels when designing and operating EMP actuators for targeted applications.

#### 4.2.4. Effect of the dimensionless electric field ( $\mu$ ) on DC dynamic response

Expanding on the previous analysis, Figs. 8(a) and (b) present the phase portraits of the actuators for various  $\mu$  values. These figures, generated with specific initial conditions ( $\nu = 1$ ,  $h = 0.5$ , and  $S = 0$ ), illustrate the DC response of the EMP actuator under a constant DC Heaviside electric signal. Fig. 8(a) reveals a noteworthy observation: as  $\mu$  increases during the suspension phase, the envelope of the thickness stretch rate exhibits a pronounced decrease. Conversely, Fig. 8(b)

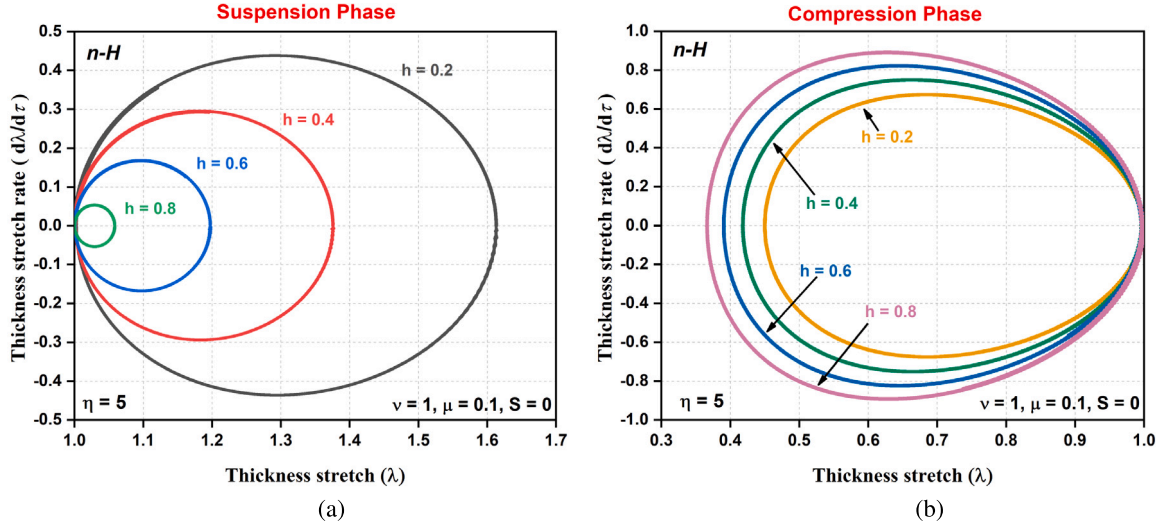


Fig. 6. DC System dynamics with varying  $h$  parameter in (a) Suspension phase (b) Compression phase.

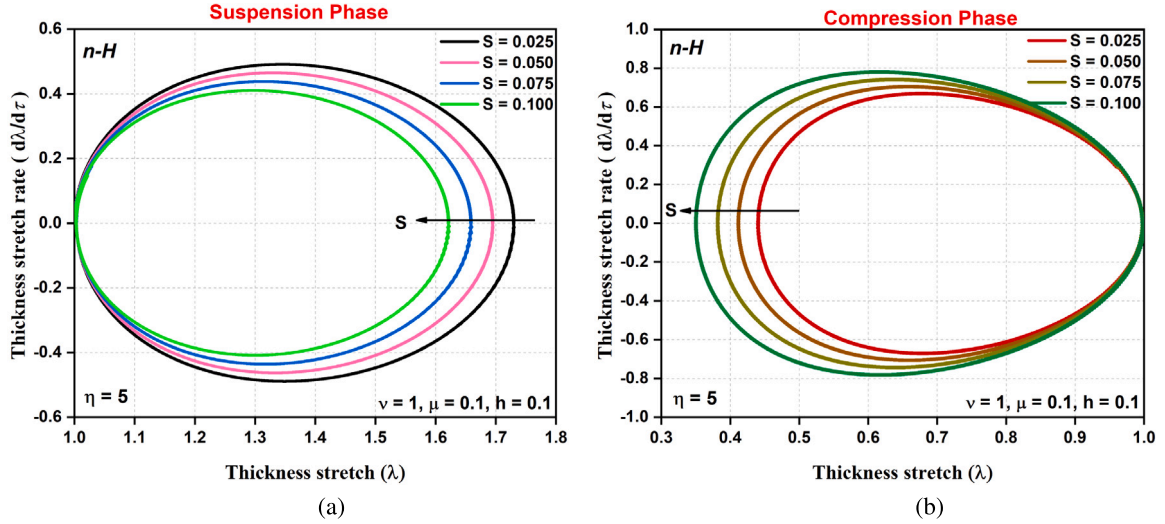


Fig. 7. DC System dynamics with varying  $S$  parameter in (a) Suspension phase (b) Compression phase.

demonstrates contrasting behavior in the compression phase. The envelope of the thickness stretch rate actually increases with increasing  $\mu$ , unlike in the suspension phase. This contrasting behavior can be attributed to the reversal of the inertial effect. During the compression phase, the electric field facilitates compression. This results in more significant deformations and, consequently, a higher envelope of the stretch rate.

Finally, when exposed to electrical stimuli, the EMAP membrane undergoes compression in alignment with the applied electric field. Beyond a specific stretch threshold, the escalation in compressive pressure surpasses the material's elastic stress rapidly, effectively counteracting the latter [56]. This heightened compressive pressure reduces the membrane thickness until structural breakdown occurs. To preempt the aforementioned instability, specific conditions are meticulously formulated. In conjunction with Refs. [57,58], Descartes's rule of sign is harnessed to define these conditions precisely. The criterion for averting static instability is derived from the equilibrium equation, wherein the Gent model is further simplified to the neo-Hookean model in the limit as  $j_m \rightarrow \infty$ . This equilibrium equation that accounts for all

the forces acting on the system is obtained from Eq. (20) as

$$(\nu + \nu\beta + h) \lambda^4 + (-1)^{p+1} \lambda^3 + (-\nu - \nu\beta + 2S) \lambda + \mu = 0. \tag{27}$$

The provided equation can have a maximum of two positive real roots. These roots determine the stability of the system in a static state: their existence ensures stability. Checking its discriminant allows us to analyze their existence. Applying this analysis to a specific case with parameters  $\nu = 1$ ,  $h = 0.1$ , and  $S = 0.1$  shows that there exists a limiting value of the control parameter  $\mu$ . For this scenario, the system demonstrates stable oscillatory behavior when  $\mu$  is less than 0.716 in the suspension phase and less than 0.17 in the compression phase. This indicates that the operational range of  $\mu$  is smaller in the compression phase than in the suspension phase, implying higher susceptibility to instability during compression. Figs. 9(a) and (b) showcase the system's behavior near the limiting  $\mu$  for both phases. As  $\mu$  approaches the limit, the system exhibits a reversal ( $\mu = 0.705$  for suspension) where its behavior changes. These phase portraits also reveal a narrowing of the phase plot approaching the limit, indicating reduced system velocity due to increased elastic energy compensating for electrostatic

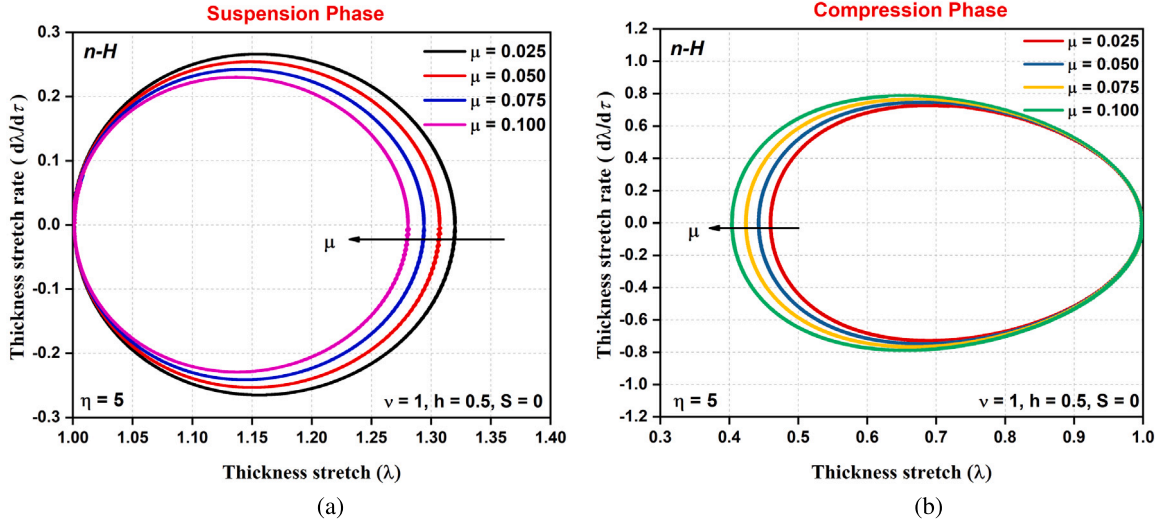


Fig. 8. DC System dynamics with varying  $\mu$  parameter in (a) Suspension phase (b) Compression phase.

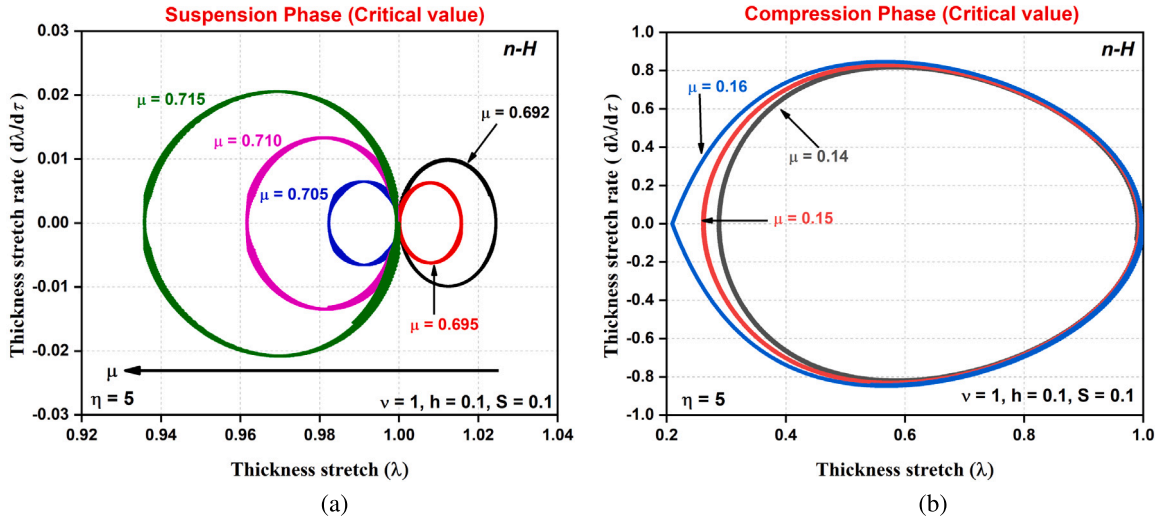


Fig. 9. Dynamic characteristics of the system as the  $\mu$  parameter approaches its critical value (a) Suspension phase (b) Compression phase.

energy. Moreover, for the suspension phase, the trend of extreme stretch difference changes upon crossing the reversal parameter value: it decreases with increasing  $\mu$  until 0.695 and then increases.

#### 4.3. AC dynamic response

The current subsection is dedicated to the examination of the nonlinear actuation characteristics of the proposed EMAP membrane under the influence of a time-dependent alternating current (AC) electric field with a harmonic nature given as [59]:

$$\mu = \mu_0 \sin(2\pi f\tau) \quad (28)$$

herein the non-dimensional excitation frequency, denoted by  $f$ , is defined as  $f = 1/\hat{\tau}$ , where  $\hat{\tau}$  represents the time period of oscillations, and  $\mu_0$  signifies the intensity of the applied alternating current (AC) electric field. By inheriting the expression of  $\mu$  from Eq. (28) and substituting Eq. (15), the ensuing nonlinear governing equation that delineates the dynamic motion of the EMAP membrane in non-dimensional form is articulated as follows:

$$\frac{d^2\lambda}{d\tau^2} + \left\{ -\nu j_m \left[ \frac{\lambda^{-2} - \lambda}{j_m - 2\lambda^{-1} - \lambda^2 + 3} \right] - \nu \beta j_m \left[ \frac{\lambda^{-2}\lambda_v - \lambda\lambda_v^{-2}}{j_m - 2\lambda^{-1}\lambda_v - \lambda^2\lambda_v^{-2} + 3} \right] \right\} = 0 \quad (29)$$

We undertake the numerical solution of the coupled differential equation (29) together with the evolution equation (20) and the specified initial conditions, delineated as follows:  $\frac{d\lambda}{d\tau}\bigg|_{\tau=0} = 0$ ;  $\lambda|_{\tau=0} = 1$ ;  $\lambda_v|_{\tau=0} = 1$ , to assess the nonlinear dynamic characteristics of the membrane subjected to an alternating current (AC) electric loading signal.

##### 4.3.1. Dimensionless parameters governing AC response

Initiating to elucidate the effect of inertial forces on the forced response of an EMAP membrane, we present time evolution diagrams, phase portraits, and Poincaré maps in Fig. 10 at a fixed dimensionless excitation frequency ( $f = 5$ ) while maintaining constant parameters ( $\nu = 1$ ,  $h = 0.1$ , and  $S = 0.1$ ). Visual examination of Fig. 10(a–b) reveals that the EMAP membrane displays oscillatory behavior gradually converging towards a stable equilibrium state throughout both the suspension and compression phases. This observed convergence can be attributed to the inherently viscoelastic character of the actuator, which dissipates the oscillations until they ultimately attain equilibrium. Noteworthy, the EMAP membrane depicted in Fig. 10(b) displays a more significant number of oscillations before achieving equilibrium relative to Fig. 10(a). This reduction in oscillations can be attributed to the

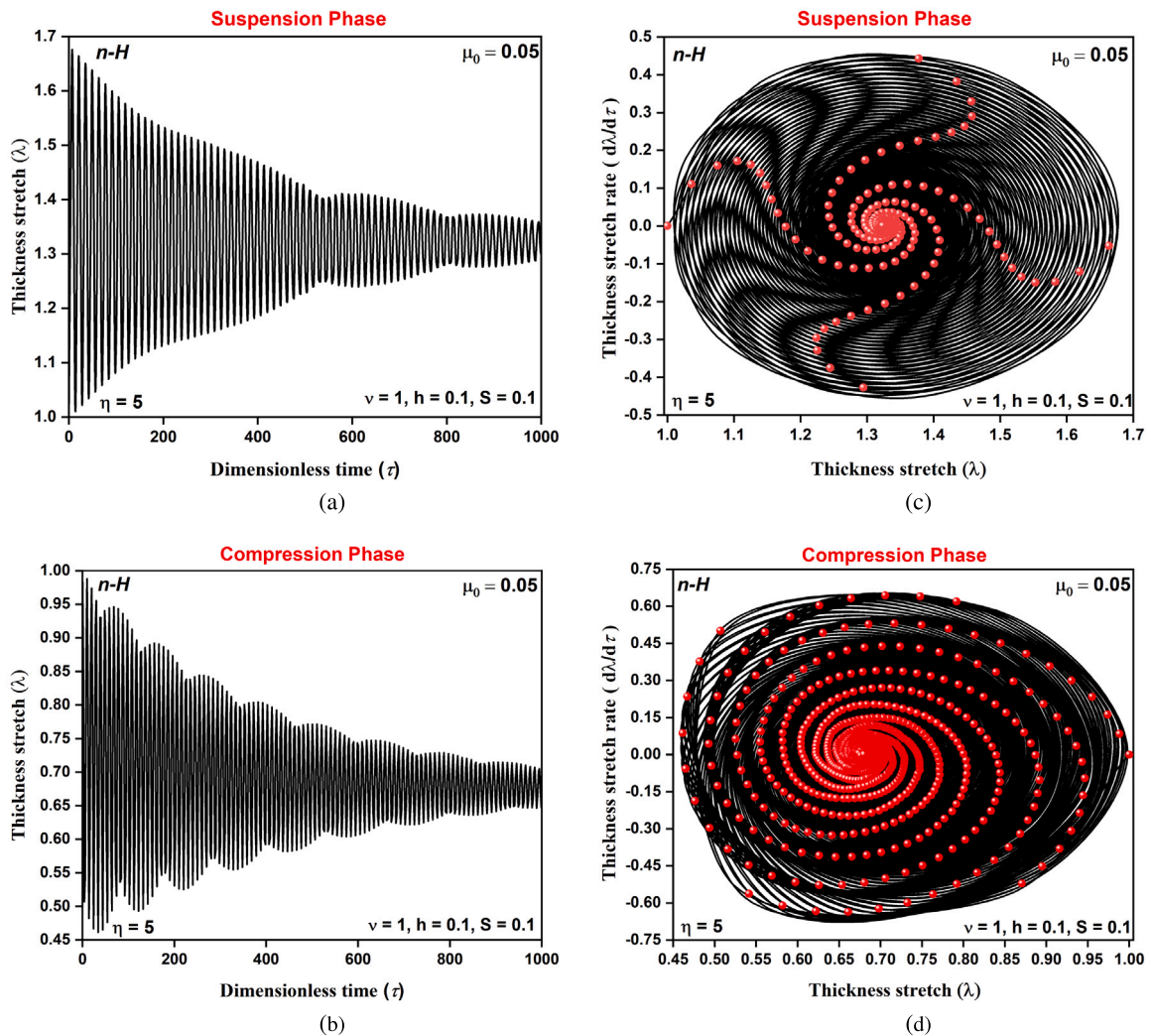


Fig. 10. Nonlinear forced responses of the EMAP actuators at suspension and compression phases. (a–b) Time evolution diagrams and (c–d) Phase portraits and Poincaré maps at excitation frequency ( $f = 5$ ).

counteraction of the electric field against the stretching action induced by the inertia in the suspension phase; conversely, the inertia now supports the compression action alongside the electric and magnetic field in the compression phase. Further, Fig. 10(c–d) present an in-depth analysis of the static oscillation characteristics of the actuators, utilizing phase portraits and Poincaré maps to provide detailed insights. These visual depictions unveil highly nonlinear oscillatory behavior, with the magnitude of these oscillations intricately linked to the direction of applied inertia within the actuator. Notably, the transition from the suspension phase to the compression phase results in a notable increase in the maximum value of the thickness stretch rate. This observation is attributed to the significant influence of inertia, which plays a pivotal role in shaping the overall dynamics of the system. Moreover, the Poincaré maps featured in Fig. 10 offer valuable information regarding the qualitative nature of the oscillations. They reveal a critical transition from quasi-periodic to periodic oscillations. This transition is not only evident in both phases but is further expedited in the compression phase. The acceleration of this transition can be comprehended by considering the reversal of the direction of the inertia effect in the compression phase, as compared to the suspension phase.

Following this, Fig. 11 illustrates time evolution diagrams, phase portraits, and Poincaré maps for two discrete values of the dimensionless magnetic parameter ( $h = 0.2$  and  $0.6$ ) at a consistent dimensionless excitation frequency ( $f = 5$ ). The parameters  $\nu = 1$ ,  $\mu = 0.1$ , and  $S$

$= 0.1$  remain constant throughout the analysis, focusing on the EMAP membrane under AC electric loading conditions. Upon visual inspection of Fig. 11(a–d), it is evident that the EMAP membranes exhibit a gradual convergence towards a stable equilibrium state. Notably, the membrane in the compression phase (Fig. 11b and d) demonstrates a higher number of oscillations before attaining equilibrium compared to the suspension phase (Fig. 11a and c). This behavior corresponds with the findings observed in Fig. 10(a) and (b). The reduction in thickness stretch with an increase in the magnetic field is attributed to the counteraction of the magnetic and electric fields against the stretching induced by inertia in the suspension phase. Conversely, the increase in the magnetic field supports the compression action. Similarly, the visual representations of the phase portraits in Fig. 11(e–h) reveal highly nonlinear oscillatory behavior, and the embedded Poincaré maps unveil a critical transition from quasi-periodic to periodic oscillations.

#### 4.3.2. Impact of excitation frequency on EMAP membrane oscillation amplitude and resonant behavior

Furthermore, we investigate the influence of excitation frequency ( $f$ ) on the amplitude of oscillation for the EMAP membrane. The amplitude is defined as half the difference between the maximum and minimum values of the thickness stretch ( $\lambda$ ). Fig. 12 depicts the relationship between amplitude and excitation frequency for various

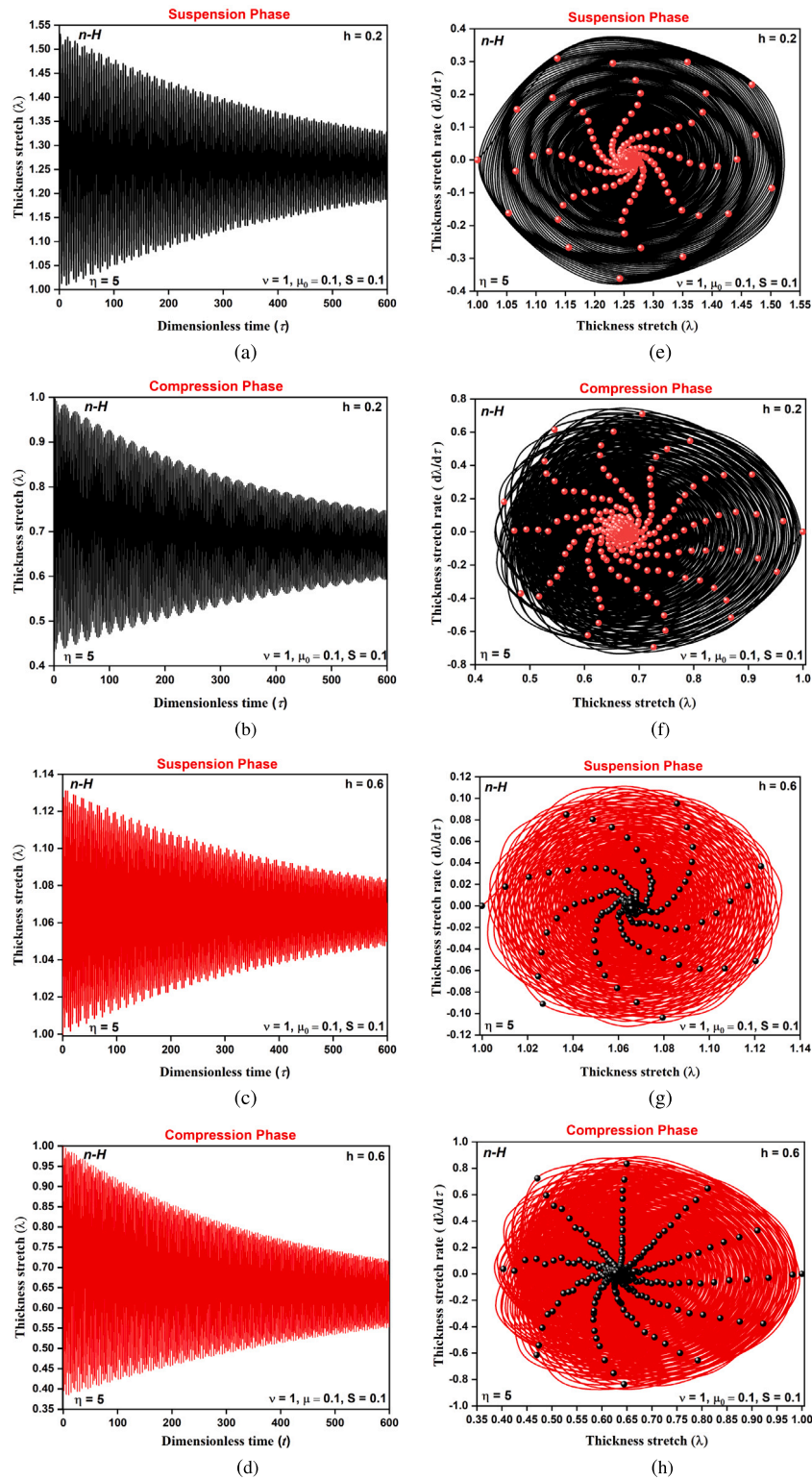


Fig. 11. Nonlinear forced responses of the EMAP actuators at suspension and compression phases at different magnetic fields  $h$ . (a–d) Time evolution diagrams and (e–h) Phase portraits and Poincaré maps at excitation frequency ( $f = 5$ ).

dimensionless electric fields ( $\mu$ ) and magnetic fields ( $h$ ) in both suspension and compression phases. As evident in Fig. 12, the oscillation amplitude reaches its maximum when the excitation frequency ( $f$ ) coincides with the natural frequency ( $f_0$ ) of the membrane. This is demonstrated in Fig. 12(a), where a peak is observed at a dimensionless frequency near 0.25. The suspension phase exhibits a direct correlation

between the electric field strength and the oscillation amplitude, as shown in Fig. 12(a). In contrast to the suspension phase, the compression phase exhibits harmonic and subharmonic resonances at excitation frequencies close to 0.8 and 2, respectively, as observed in Fig. 12(b). These curves suggest that AC dynamic instability is triggered near these specific frequencies due to significant membrane deformation,

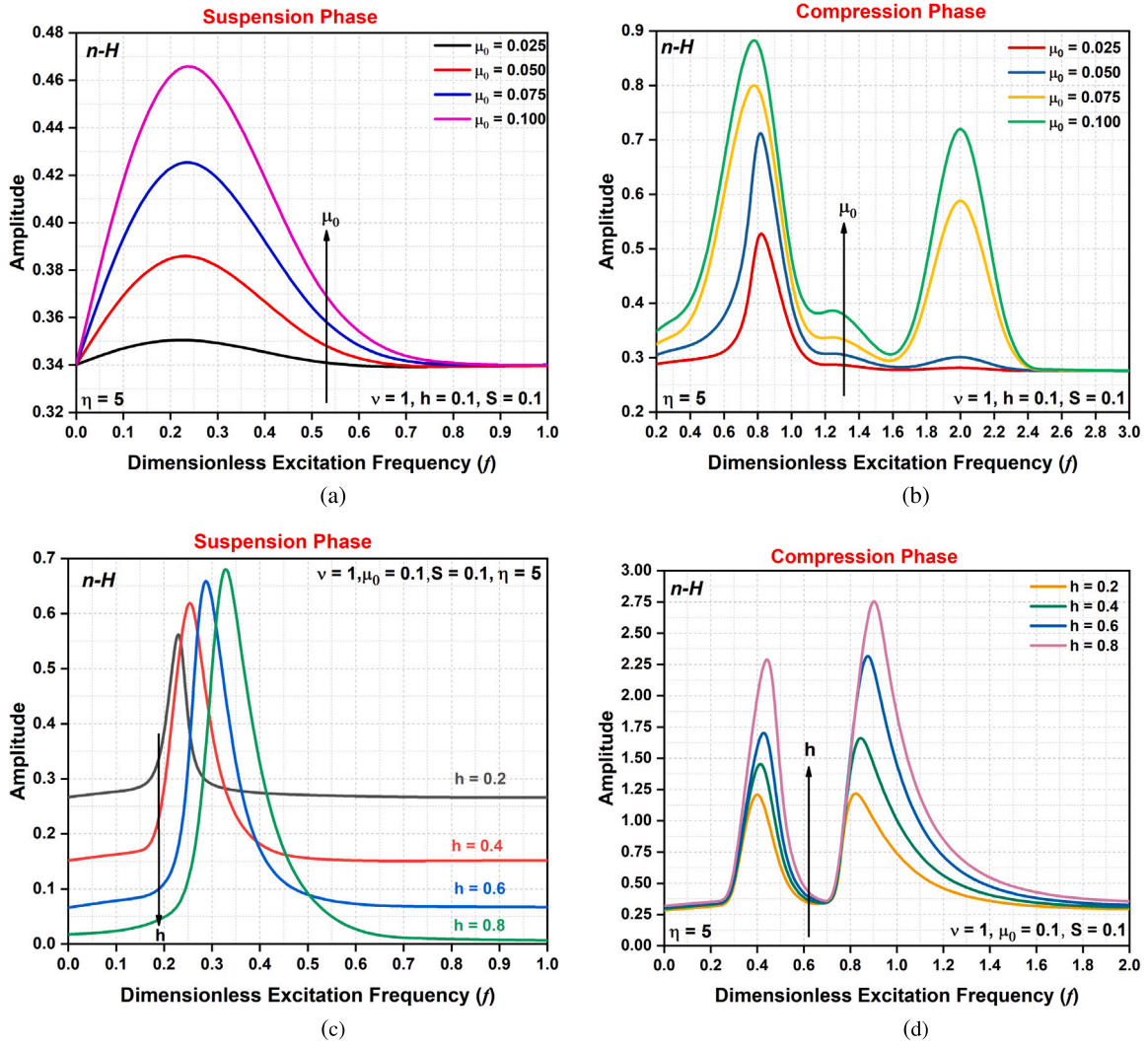


Fig. 12. Variation of applied excitation frequency with thickness stretch amplitude for EMAP ( $\eta = 5$ ) actuators. (a–b) Different intensities of electric field ( $\mu_0$ ). (c–d) Different magnetic fields ( $h$ ).

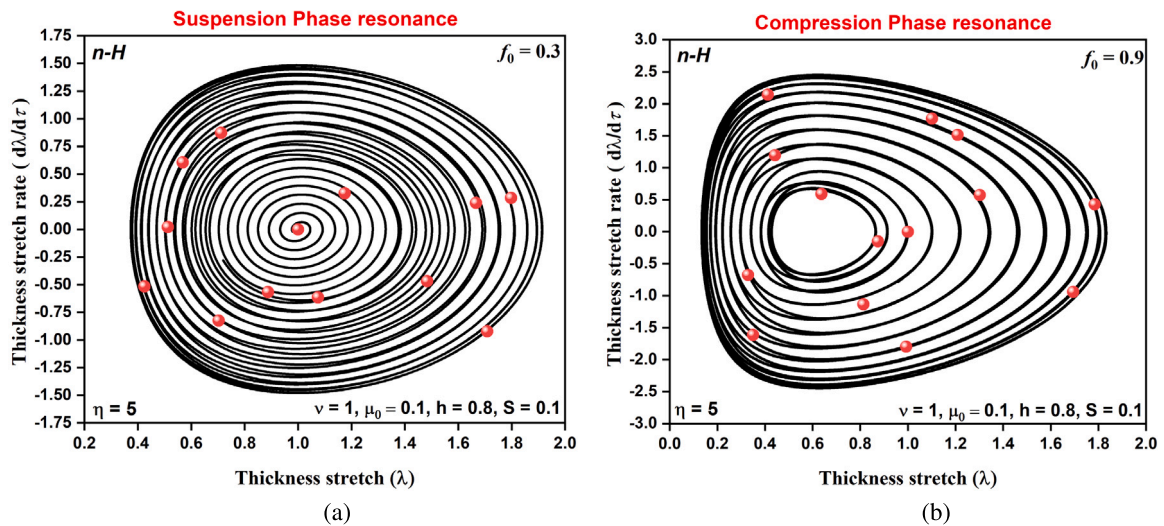


Fig. 13. Phase portraits and Poincaré maps of EMAP Actuators with Viscosity Parameter  $\eta = 5$  under harmonic excitation in (a) Suspension phase (b) Compression phase.

as referenced in previous work [51,60]. Fig. 12(c) illustrates that increasing the dimensionless magnetic field ( $h$ ) in the suspension phase

intensifies both the resonant frequencies and the vibration intensity. Interestingly, Fig. 12(d) reveals that the compression phase membrane

also exhibits peaks at an excitation frequency close to 0.4, categorized as superharmonic resonance [18,61–63]. Similar to the suspension phase, the amplitude of these superharmonic and harmonic resonances also increases with increasing  $h$  in the compression case.

In conclusion, we present phase portraits and Poincaré maps to analyze the nonlinear oscillatory response of the EMAP actuator ( $\eta = 5$ ) excited by resonant frequencies of  $f_0 = 0.3$  and  $0.9$  for the suspension and compression phases, respectively, as depicted in Fig. 13. The figures illustrate that resonance induces deviations in the typical oscillation behavior, leading to the formation of closed spirals. Additionally, the Poincaré maps for both scenarios display isolated points, indicating stable periodic oscillations and highlighting the resonant behavior of the actuators.

## 5. Concluding remarks

Most current dynamic studies of electromagnetoactive polymeric (EMAP) membranes rely on the hypothesis that electrodes are massless. However, the electrodes can possess much higher inertia in comparison to the elastomeric membranes. To closely mimic their actual behavior, we have proposed a model for the nonlinear axial oscillation of the EMAP membrane that includes electrode inertia. Using the neo-Hookean material model (equivalent to the higher value of chain extensibility parameter in the chosen Gent material model) to generalize the analysis for both the suspension and compression phases leads to the following significant findings:

### 5.1. Static stretch and natural frequency:

- i. Critical electric field parameter ( $\mu$ ) thresholds exist for instability in both suspension and compression phases.
- ii. Increasing electrode inertia ( $\nu$ ) initially reduces, then increases, the maximum stable  $\mu$  in suspension.
- iii. Higher  $\nu$  leads to higher stable  $\mu$  and natural frequency in compression.
- iv. Magnetic field parameter ( $h$ ) improves stability by lowering the maximum  $\mu$  threshold.

### 5.2. DC dynamic response:

- i. Electrode inertia ( $\nu$ ) reduces energy storage due to lower extreme stretches.
- ii. Magnetic field ( $h$ ) dissipates energy in suspension but stores energy in compression.
- iii. Prestress ( $S$ ) reduces energy in suspension but increases compression.
- iv. The electric field decreases the stretch rate in suspension while increasing compression, with stability analysis revealing critical values that cause behavior reversal and reduced system velocity near the transition point.

### 5.3. AC dynamic response:

- i. The study reveals oscillatory behavior in EMAP membranes transitioning towards stable equilibrium states due to their viscoelastic nature.
- ii. The compression phase displays more oscillations before reaching equilibrium than the suspension phase, influenced by inertia ( $h$ ) and the interplay of the electric field ( $\mu$ ).
- iii. Due to inertial impact, moving from suspension to compression phases significantly boosts the maximum thickness stretch rate.
- iv. Poincaré maps illustrate a critical shift from quasi-periodic to periodic oscillations both in suspension and compression phases.

- v. The suspension phase links electric field strength to oscillation amplitude, with harmonic and subharmonic resonances in compression potentially causing instabilities; increasing the magnetic field intensifies resonant frequencies and vibrations, leading to variations in oscillation patterns, as seen in closed spirals in phase portraits and validated by Poincaré maps.

These thorough results offer insightful information on how to develop and operate EMAP membrane-based actuators and comprehend how various parameters affect stability and dynamic response during both the suspension and compression phases. The current analytical findings will be validated experimentally in a separate communication in the near future.

## CRedit authorship contribution statement

**Ashesh Kumar Patra:** Writing – original draft, Validation, Software, Methodology, Investigation, Formal analysis, Data curation, Conceptualization. **Aman Khurana:** Writing – review & editing, Supervision, Resources, Methodology, Investigation, Funding acquisition, Formal analysis, Conceptualization. **Deepak Kumar:** Writing – review & editing, Validation, Supervision, Methodology, Investigation, Formal analysis, Conceptualization. **Prashant Saxena:** Writing – review & editing, Writing – original draft, Visualization, Supervision, Project administration, Funding acquisition.

## Declaration of competing interest

The authors declare that they have no known competing financial interests or personal relationships that could have appeared to influence the work reported in this paper.

## Data availability

No data was used for the research described in the article.

## Acknowledgments

Aman Khurana acknowledges the financial support provided by the Department of Science and Technology (DST), Government of India through Grant No. DST/INSPIRE/04/2022/001174 and the Indian Institute of Technology Indore, India through the “Young Research Seed Grant Scheme”. Prashant Saxena acknowledges the support of Engineering and Physical Sciences Research Council, United Kingdom through the project no. EP/V030833/1.

## References

- [1] K. Petcharoen, A. Sirivat, Magneto-electro-responsive material based on magnetite nanoparticles/polyurethane composites, *Mater. Sci. Eng. C* 61 (2016) 312–323.
- [2] C. Miehe, D. Vallicotti, S. Teichtmeister, Homogenization and multiscale stability analysis in finite magneto-electro-elasticity. Application to soft matter EE, ME and MEE composites, *Comput. Methods Appl. Mech. Engrg.* 300 (2016) 294–346.
- [3] O. Araromi, A. Conn, C. Ling, J. Rossiter, R. Vaidyanathan, S. Burgess, Spray deposited multilayered dielectric elastomer actuators, *Sensors Actuators A* 167 (2011) 459–467.
- [4] S.K. Behera, D. Kumar, C.S. Maurya, S. Sarangi, Universal rate-dependence in electro-magneto-active polymeric composites, *Compos. Sci. Technol.* 237 (2023) 110015.
- [5] A.K. Patra, A.K. Sharma, D. Joglekar, M.M. Joglekar, Propagation of the fundamental lamb modes in strain stiffened hard-magnetic soft plates, *J. Appl. Mech.* (2024) 1–26.
- [6] A.K. Patra, A. Khurana, D. Kumar, Modeling and analysis of a thermo-electro-magneto-viscoelastic actuator, *Int. J. Appl. Mech.* (2023).
- [7] D. Kumar, S. Sarangi, Constitutive modeling of an electro-magneto-rheological fluid, *Sci. Rep.* 12 (1) (2022) 4584.
- [8] A. Khurana, D. Kumar, A.K. Sharma, M.M. Joglekar, Nonlinear oscillations of particle-reinforced electro-magneto-viscoelastomer actuators, *J. Appl. Mech.* 88 (12) (2021) 121002.

- [9] W. Yuan, T.L. Lam, J. Biggs, B. Chen, Q.B.P.G. Gruner, Q.B. Pei, Fault-tolerant dielectric elastomer actuators using single-walled carbon nanotube electrodes, *Adv. Mater.* 20 (2008) 621–625.
- [10] K. Ren, S. Liu, M. Lin, Y. Wang, Q. Zhang, A compact electroactive polymer actuator suitable for refreshable braille display, *Sensors Actuators A* 143 (2) (2008) 335–342.
- [11] K. Arya, D. Kumar, S. Sarangi, Free radial oscillations of an actuated cylindrical tube, *Mech. Adv. Mater. Struct.* (2022) 1–11.
- [12] A. Khurana, S. Naskar, R. Varma, T. Mukhopadhyay, Smart electro-magneto-viscoelastomer minimum energy structures with particle-reinforcements: Theoretical equilibrium and nonlinear dynamics of actuated configurations, *Internat. J. Engrg. Sci.* 194 (2024) 103974.
- [13] D. Kumar, S. Sarangi, R. Bhattacharyya, Universal relations in nonlinear electro-magneto-elasticity, *Arch. Appl. Mech.* 90 (2020) 1643–1657.
- [14] D. Kumar, S. Ghosh, S. Roy, S. Santapuri, Modeling and analysis of an electro-pneumatic braided muscle actuator, *J. Intell. Mater. Syst. Struct.* 32 (4) (2021) 399–409.
- [15] R.A. Ranjan, S. Sarangi, Effect of electrode on the dynamics of electroactive membrane, *J. Appl. Mech.* (2023) 1–11.
- [16] D. Kumar, S. Sarangi, Instability analysis of an electro-magneto-elastic actuator: A continuum mechanics approach, *AIP Adv.* 8 (11) (2018).
- [17] S. Rosset, H.R. Shea, Flexible and stretchable electrodes for dielectric elastomer actuators, *Appl. Phys. A* 110 (2013) 281–307.
- [18] J. Zhu, S. Cai, Z. Suo, Resonant behavior of a membrane of a dielectric elastomer, *Int. J. Solids Struct.* 47 (24) (2010) 3254–3262.
- [19] F. Carpi, P. Chiarelli, A. Mazzoldi, D. De Rossi, Electromechanical characterisation of dielectric elastomer planar actuators: comparative evaluation of different electrode materials and different counterloads, *Sensors Actuators A* 107 (1) (2003) 85–95.
- [20] T.P. Willian, B. Fasolt, P. Motzki, G. Rizzello, S. Seelecke, Effects of electrode materials and compositions on the resistance behavior of dielectric elastomer transducers, *Polymers* 15 (2) (2023) 310.
- [21] Y. Qiu, E. Zhang, R. Plamthottam, Q. Pei, Dielectric elastomer artificial muscle: materials innovations and device explorations, *Acc. Chem. Res.* 52 (2) (2019) 316–325.
- [22] H. Park, T. Nguyen, Viscoelastic effects on electromechanical instabilities in dielectric elastomers, *Soft Matter* 9 (2013) 1031–1042.
- [23] J. Wang, T.D. Nguyen, H.S. Park, Electrostatically driven creep in viscoelastic dielectric elastomers, *J. Appl. Mech.* 81 (2014) 051006.
- [24] A. Kumar, A. Khurana, A.K. Sharma, M. Joglekar, Dynamics of pneumatically coupled visco-hyperelastic dielectric elastomer actuators: Theoretical modeling and experimental investigation, *Eur. J. Mech. A Solids* 95 (2022) 104636.
- [25] P. Saxena, D. Khoi Vu, P. Steinmann, On rate-dependent dissipation effects in electro-elasticity, *Int. J. Non-Linear Mech.* 62 (2014) 1–11.
- [26] L.J. Romasanta, M.A. López-Manchado, R. Verdejo, Increasing the performance of dielectric elastomer actuators: A review from the materials perspective, *Prog. Polym. Sci.* 51 (2015) 188–211.
- [27] A. Khurana, D. Kumar, A.K. Sharma, M. Joglekar, Static and dynamic instability modeling of electro-magneto-active polymers with various entanglements and crosslinks, *Int. J. Non-Linear Mech.* 139 (2022) 103865.
- [28] A.K. Patra, A. Khurana, D. Kumar, Modeling and analysis of a thermo-electro-magneto-viscoelastic actuator, *Int. J. Appl. Mech.* 16 (02) (2024) 2450015.
- [29] Z. Suo, X. Zhao, W. H. Greene, A nonlinear field theory of deformable dielectrics, *J. Mech. Phys. Solids* 56 (2008) 467–486.
- [30] L. Dorfmann, R.W. Ogden, *Nonlinear Theory of Electroelastic and Magnetoelastic Interactions*, Springer, 2014.
- [31] D. Kumar, S. Sarangi, P. Saxena, Universal relations in coupled electro-magneto-elasticity, *Mech. Mater.* 143 (2020) 103308.
- [32] D. Kumar, V. Yadav, S. Sarangi, Modeling and analysis of an electro-magneto-elastic rotating cylindrical tube actuator, *J. Intell. Mater. Syst. Struct.* 33 (14) (2022) 1862–1876.
- [33] R.M. McMeeking, C.M. Landis, S. M.A. Jimenez, A principle of virtual work for combined electrostatic and mechanical loading of materials, *Int. J. Non-Linear Mech.* 42 (2007) 831–838.
- [34] B.L. Sharma, P. Saxena, Variational principles of nonlinear magnetoelastostatics and their correspondences, *Math. Mech. Solids* 26 (2021) 1424–1454.
- [35] P. Saxena, B.L. Sharma, On equilibrium equations and their perturbations using three different variational formulations of nonlinear electroelastostatics, *Math. Mech. Solids* 25 (8) (2020) 1589–1609.
- [36] Y.-X. Xie, J.-C. Liu, Y. Fu, Bifurcation of a dielectric elastomer balloon under pressurized inflation and electric actuation, *Int. J. Solids Struct.* 78–79 (2016) 182–188.
- [37] A. Khurana, M. Joglekar, G. Zurlo, Electromechanical stability of wrinkled dielectric elastomers, *Int. J. Solids Struct.* 246 (2022) 111613.
- [38] P. Saxena, N.H. Reddy, S.P. Pradhan, Magnetoelastic deformation of a circular membrane: Wrinkling and limit point instabilities, *Int. J. Non-Linear Mech.* 116 (2019) 250–261.
- [39] Z. Liu, A. McBride, B.L. Sharma, P. Steinmann, P. Saxena, Coupled electro-elastic deformation and instabilities of a toroidal membrane, *J. Mech. Phys. Solids* (2021) 104221.
- [40] A. Khurana, D. Kumar, A.K. Sharma, G. Zurlo, M. Joglekar, Taut domains in transversely isotropic electro-magneto-active thin membranes, *Int. J. Non-Linear Mech.* 147 (2022) 104228.
- [41] S. Soni, N. Jain, P. Joshi, Analytical modeling for nonlinear vibration analysis of partially cracked thin magneto-electro-elastic plate coupled with fluid, *Nonlinear Dynam.* 90 (2017) 137–170.
- [42] V. Settini, F. Romeo, Dynamic regimes of a nonlinearly coupled electromechanical system, *Int. J. Non-Linear Mech.* 103 (2018) 68–81.
- [43] H. Jafari, R. Sedaghati, Free and forced vibration behaviors of magnetodielectric effect in magnetorheological elastomers, *Vibration* 6 (1) (2023) 269–285.
- [44] L. Chen, X. Yang, B. Wang, S. Yang, Nonlinear electromechanical coupling in graded soft materials: Large deformation, instability, and electroactuation, *Phys. Rev. E* 102 (2) (2020) 023007.
- [45] A.K. Sharma, A. Khurana, M.M. Joglekar, A finite element model for investigating the thermo-electro-mechanical response of inhomogeneously deforming dielectric elastomer actuators, *Eur. J. Comput. Mech.* (2021) 387–408.
- [46] K. Volokh, On electromechanical coupling in elastomers, 2012.
- [47] F. Ebrahimi, M.R. Barati, Dynamic modeling of magneto-electrically actuated compositionally graded nanosize plates lying on elastic foundation, *Arab. J. Sci. Eng.* 42 (5) (2017) 1977–1997.
- [48] A. Khurana, A. Kumar, S.K. Raut, A.K. Sharma, M.M. Joglekar, Effect of viscoelasticity on the nonlinear dynamic behavior of dielectric elastomer minimum energy structures, *Int. J. Solids Struct.* 208 (2021) 141–153.
- [49] A. Kumar, A. Khurana, A.K. Sharma, M. Joglekar, An equivalent spring-based model to couple the motion of visco-hyperelastic dielectric elastomer with the confined compressible fluid/air mass, *Int. J. Non-Linear Mech.* 147 (2022) 104232.
- [50] K. Kashyap, A.K. Sharma, M.M. Joglekar, Nonlinear dynamic analysis of anisovisco-hyperelastic dielectric elastomer actuators, *Smart Mater. Struct.* 29 (5) (2020) 055014.
- [51] A. Khurana, A.K. Sharma, M.M. Joglekar, Nonlinear oscillations of electrically driven aniso-visco-hyperelastic dielectric elastomer minimum energy structures, *Nonlinear Dynam.* 104 (3) (2021) 1991–2013.
- [52] J. Wang, T.D. Nguyen, H.S. Park, Electrostatically driven creep in viscoelastic dielectric elastomers, *J. Appl. Mech.* 81 (5) (2014) 051006.
- [53] P. Brochu, Q. Pei, Dielectric elastomers for actuators and artificial muscles, *Electroact. Polym. Mater.* (2012) 1–56.
- [54] A. Iannarelli, M.G. Niasar, R. Ross, The effects of static pre-stretching on the short and long-term reliability of dielectric elastomer actuators, *Smart Mater. Struct.* 28 (12) (2019) 125014.
- [55] R. Aditi Ranjan, S. Sarangi, Effect of electrode on the dynamics of electroactive membrane, *J. Appl. Mech.* 91 (2) (2024).
- [56] R.E. Pelrine, R.D. Kornbluh, J.P. Joseph, Electrostriction of polymer dielectrics with compliant electrodes as a means of actuation, *Sensors Actuators A* 64 (1) (1998) 77–85.
- [57] E. Rees, Graphical discussion of the roots of a quartic equation, *Amer. Math. Monthly* 29 (2) (1922) 51–55.
- [58] S. Janson, Resultant and discriminant of polynomials, 2007, Notes, September 22.
- [59] A. Kumar, A. Khurana, A.K. Patra, Y. Agrawal, M. Joglekar, Electromechanical performance of dielectric elastomer composites: Modeling and experimental characterization, *Compos. Struct.* 320 (2023) 117130.
- [60] A. Khurana, A. Kumar, A.K. Sharma, M. Joglekar, Effect of polymer chains entanglements, crosslinks and finite extensibility on the nonlinear dynamic oscillations of dielectric viscoelastomer actuators, *Nonlinear Dynam.* 104 (2) (2021) 1227–1251.
- [61] H.-I. Dai, L. Wang, Nonlinear oscillations of a dielectric elastomer membrane subjected to in-plane stretching, *Nonlinear Dynam.* 82 (2015) 1709–1719.
- [62] A.H. Nayfeh, D.T. Mook, *Nonlinear Oscillations*, John Wiley & Sons, 2008.
- [63] H. Vatanjou, Y. Hojjat, M. Karafi, Nonlinear dynamic analysis of dielectric elastomer minimum energy structures, *Appl. Phys. A* 125 (2019) 1–11.